ACS NANO
Cite This: ACS Nano 2017, 11, 9979-9988
www.acsnano.org

ARTICLE

Upconversion Nanoparticles/Hyaluronate–Rose Bengal Conjugate Complex for Noninvasive Photochemical Tissue Bonding

Seulgi Han,[†] Byung Woo Hwang,[†] Eun Young Jeon,[‡] Dooyup Jung,[‡] Geon Hui Lee,[†] Do Hee Keum,[†] Ki Su Kim,[*,§,⊥,∥] Seok Hyun Yun,[⊥] Hyung Joon Cha,[‡] and Sei Kwang Hahn[*,†,§]

[†]Department of Materials Science and Engineering, Pohang University of Science and Technology (POSTECH), 77 Cheongam-ro, Nam-gu, Pohang, Gyeongbuk 37673, Korea

[‡]Department of Chemical Engineering, Pohang University of Science and Technology (POSTECH), 77 Cheongam-ro, Nam-gu, Pohang, Gyeongbuk 37673, Korea

[§]PHI BIOMED Co., #613, 12 Gangnam-daero 65-gil, Seocho-gu, Seoul 06612, Korea

[⊥]Wellman Center for Photomedicine, Harvard Medical School and Massachusetts General Hospital, 65 Landsdowne Street UP-5, Cambridge, Massachusetts 02139, United States

ABSTRACT: **The recent progress in photonic nanomaterials has contributed greatly to the development of photomedicines. However, the finite depth of light penetration is still a serious limitation, constraining their clinical applications. Here, we developed a poly(allylamine) (PAAm)-modified upconversion nanoparticle/hyaluronate–rose bengal (UCNP/PAAm/HA-RB) conjugate complex for photochemical bonding of deep tissue with near-infrared (NIR) light illumination. Compared to the conventional invasive treatment *via* suturing and stapling, the UCNP/PAAm/HA-RB conjugate complex could be noninvasively delivered into the deep tissue and accelerate the tissue bonding upon NIR light illumination. HA in the outer layer of the complex facilitated the penetration of RB into the collagen layer of the dermis. The NIR light triggered UCNP of $NaYF_4$:Yb/Er (Y:Yb:Er = 78:20:2) in the complex to illuminate visible green light under the skin tissue. The activated RB in the HA-RB conjugate by the green light induced radical formation for the cross-linking of incised collagen matrix. An *in vitro* light propagation test and collagen fibrillogenesis analysis, an *in vivo* animal tissue bonding test, and an *ex vivo* tensile strength test of dissected skin tissues confirmed the successful photochemical tissue bonding effect of the UCNP/PAAm/HA-RB conjugate complex.**

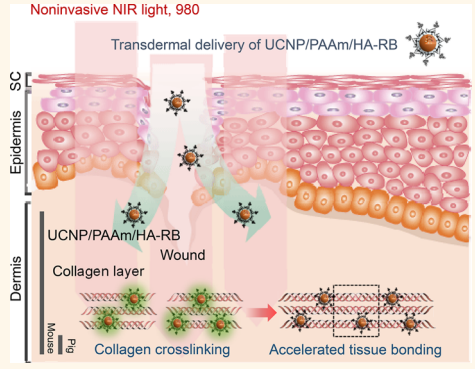

KEYWORDS: *upconversion nanoparticle, hyaluronate, rose bengal, near-infrared light, tissue bonding*

Photomedicine is a future technology using light for diverse biomedical applications to dermatology, laser surgery, optical diagnosis, and cancer therapy. Among these applications, photochemical tissue bonding (PTB) is a dye-assisted photochemical technique for wound closure.[1] This technique has been regarded as an effective alternative to stapling or traditional suturing. It can be exploited for futuristic robot surgery due to facile and quick tissue bonding triggered by light with reduced scar formation and secondary inflammation.[2] Rose bengal (RB) dye induces the cross-linking of the collagen matrix in damaged skin tissue for nanosuturing. Green light at a wavelength of *ca.* 540 nm activates the RB to take an electron from the collagen, making a free radical. Then, the collagen matrix can be knitted back together for the tissue bonding.[3] In our previous work, we have developed biodegradable polymeric waveguides to transport light efficiently into deep tissue and induce the activation of RB for PTB.[4] However, this method required invasive implantation or injection for the application of polymeric waveguides.

Upconversion nanoparticles (UCNPs) can be used as a facile light source platform for various photomedicines to replace the conventional implantable and injectable light-guiding materials. UCNPs have the unique optical property of photon upconversion in the electromagnetic spectrum to convert the tissue-penetrating near-infrared (NIR) light to visible light, enabling biophotonic applications in deep tissue. UCNPs consist of lanthanide (Ln)- or actinide-doped transition metals for the host lattice, activator ions, and sensitizer ions. The phase and size of UCNPs can be tuned by changing the doping concentration[5] and the synthetic condition.[6] The lifetime of

Received: June 14, 2017
Accepted: September 11, 2017
Published: September 11, 2017

DOI: 10.1021/acsnano.7b04153
ACS Nano 2017, 11, 9979–9988

fluorescence[7] and the multicolor output[8] can be controlled by changing the doped Ln composition and the synthesis temperature. UCNPs have been widely investigated for a variety of biomedical applications including multimodal bioimaging,[9,10] photodynamic therapy,[11,12] and photothermal therapy.[13]

Here, we developed a versatile deep tissue photomedicine of poly(allylamine) (PAAm)-modified upconversion nanoparticle/hyaluronate−rose bengal (UCNP/PAAm/HA-RB) conjugate complex for PTB *via* transdermal delivery (Figure 1).

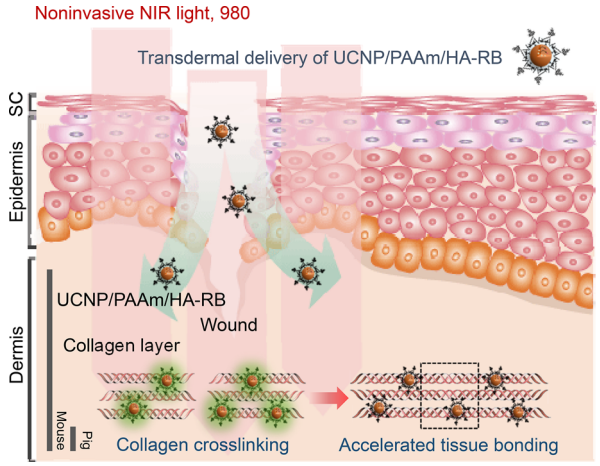

Figure 1. Schematic illustration for photochemical tissue bonding of incised collagen matrix by near-infrared light illumination after transdermal delivery of polyallylamine (PAAm)-modified upconversion nanoparticle/hyaluronate−rose bengal (UCNP/PAAm/HA-RB) conjugate complex (gray scale bars = 100 μm, SC: stratum corneum).

HA has been widely investigated as a promising transdermal delivery carrier for protein drugs[14] and nanomaterials including nanographene oxide[15] and carbon dots.[16] The hygroscopic HA can hydrate the skin barrier and penetrate through the skin due to the hydrophobic patch domain in the HA backbone.[17] The highly expressed HA receptors in skin tissues can also facilitate the transdermal delivery of HA. As schematically shown in Figure 1, the UCNP/PAAm/HA-RB conjugate complex can be transdermally delivered into a deep and wide area from the boundary of incision due to HA in the outer layer. Upon NIR light illumination, UCNP can convert the NIR to green light for the activation of RB in the HA-RB conjugate, inducing collagen cross-linking for accelerated sutureless tissue bonding. After *in vitro* characterization of the UCNP/PAAm/HA-RB conjugate complex, we have successfully demonstrated the effective PTB *via in vivo* and *ex vivo* tissue bonding tests.

RESULTS AND DISCUSSION

Synthesis and Characterization of the UCNP/PAAm/HA-RB Conjugate Complex. For the PTB in deep tissues by upconversion of NIR light to visible green light, the UCNPs were synthesized at a high temperature of 300 °C. The surface of the UCNPs was modified with PAAm by the ligand-exchange method to provide the hydrophilicity and positive charge (Figure 2a). According to high-resolution transmission electron microscopy (HRTEM) and X-ray diffraction (XRD) spectroscopy, UCNPs appeared to have a (100) hexagonal crystal lattice with a uniform size of 30.43 ± 2.10 nm (Figure 2b). The composition of the UCNPs was 78:19:3 of Y:Yb:Er in the energy dispersive spectroscopy (EDS) (Figure 2c) and 77:21:2 of Y:Yb:Er in the inductively coupled plasma optical emission spectrometry (ICP-OES). The composition of UCNPs was averaged to 78:20:2 of Y:Yb:Er, which did match well with the used amount of Ln precursors. At this composition, the quantum yield of UCNPs is typically regarded as *ca.* 0.3% as reported elsewhere.[18−21] Accordingly, the intensity of converted green light by UCNPs was estimated to be *ca.* 1.5 mW/cm^2 under 980 nm NIR light (500 mW/cm^2) illumination. The fluorescence of UCNPs in cyclohexane, UCNP/PAAm, and UCNP/PAAm/HA-RB conjugate complex dissolved in distilled (DI) water appeared to be almost the same at 540 nm (Figure 2d).

Meanwhile, HA-RB conjugate was synthesized by the coupling reaction between carboxyl groups of the RB and amine groups of diaminohexane (DAH)-HA *via* the EDC/NHS chemistry. The successful synthesis of the HA-RB conjugate was confirmed from the peak shift of the absorbance spectra in Figure 3a.[22] The absorbance peak of the HA-RB conjugate was shifted to 570 nm, whereas those of the RB and HA-DAH+RB mixture were shown at 550 nm. The UCNP/PAAm/HA-RB conjugate complex was formed by the electrostatic interaction between positively charged UCNP/PAAm and negatively charged HA-RB conjugate. UV/vis spectrophotometry and fluorometry showed the overlap between the absorbance wavelength of the HA-RB conjugate and the emission wavelength of UCNP/PAAm, indicating that the HA-RB conjugate can be activated by green light converted by UCNP upon NIR light illumination (Figure 3b). Dynamic light scattering (DLS) and zeta potential analysis revealed the size reduction of the UCNP/PAAm/HA-RB conjugate complex to 459.9 ± 98 nm after mixing of UCNP/PAAm with the HA-RB conjugate (Figure 3c). The zeta potential of the UCNP/PAAm/HA-RB conjugate complex was shifted to the stable value of −27 ± 0.42 mV as shown in Figure 3d. All these results confirmed the successful preparation of the UCNP/PAAm/HA-RB conjugate complex.

Before assessing the effect of the UCNP/PAAm/HA-RB conjugate complex on the PTB, we investigated the cytotoxicity of RB, HA-RB conjugate, UCNP/PAAm, and the UCNP/PAAm/HA-RB conjugate complex in NIH 3T3 cells (mouse fibroblast) by the MTT assay (Figure 3e and f). The cell viability test revealed that HA contributed to improve the biocompatibility of the conjugated or complexed materials. After incubation for a day, relative cell viability treated by both RB and HA-RB conjugate decreased with increasing concentration of RB (Figure 3e). However, the HA-RB conjugate showed a lower cytotoxicity than that of RB, maintaining over 80% of cell viability at the RB concentration of 1000 μM. In addition, both UCNP/PAAm and the UCNP/PAAm/HA-RB conjugate complex showed a decrease of relative cell viability with increasing concentration of UCNP/PAAm (Figure 3f). Nevertheless, the UCNP/PAAm/HA-RB conjugate complex appeared to be more biocompatible than UCNP/PAAm because of the electrostatic neutralization between the negatively charged HA-RB conjugate and positively charged UCNP/PAAm. The cell viability was maintained over 90% at the UCNP/PAAm concentration of 200 μg/mL.

Light Propagation into Closed Incision of Porcine Tissue. To assess the light delivery efficiency of the UCNP/PAAm/HA-RB conjugate complex into the tissue, a light propagation test was performed using porcine skin tissues with a similar tissue structure and thickness to human skin.[23] As

DOI: 10.1021/acsnano.7b04153
ACS Nano 2017, 11, 9979−9988

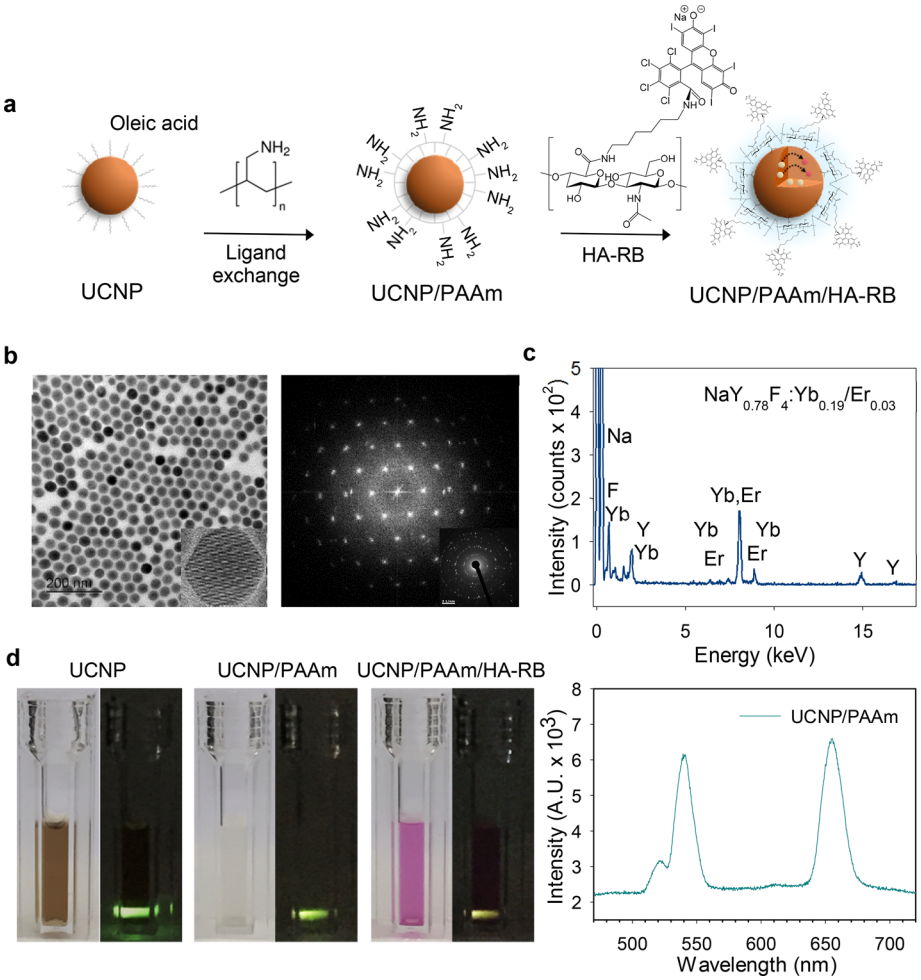

Figure 2. Preparation and characterization of the UCNP/PAAm/HA-RB conjugate complex. (a) Schematic illustration for the synthesis of UCNP/poly(allylamine) (PAAm) by ligand exchange and the preparation of UCNP/PAAm/HA-RB conjugate complex by electrostatic interaction between UCNP/PAAm and HA-RB conjugate. (b) TEM and XRD images for the uniform crystal lattice of UCNPs. (c) EDS for the composition of UCNPs. (d) Fluorescence of UCNP, UCNP/PAAm, and UCNP/PAAm/HA-RB conjugate complex and photoluminescence intensity of UCNP/PAAm.

shown in Figure 4a, the green laser could not reach into the dermis layer, but was scattered in the stratum corneum (SC) layer. On the other hand, the NIR laser penetrated into the dermal layer of skin tissue treated with the complex for 30 min and converted to green light by UCNPs in the complex. Figure 4b shows the analysis for the light propagation of green laser and green light from the complex. In the direction of *X*-axis, the green light triggered by the NIR laser was spread in the bigger area and showed a stronger intensity at 540 nm than the green laser. In the direction of the *Z*-axis, the intensity$_{540\ nm}$ of the green light from the complex was strongly detected at a depth of *ca.* 1.5 mm, whereas the intensity$_{540\ nm}$ of the green laser was dramatically decreased below the depth of *ca.* 0.25 mm (only SC layer). In addition, two-photon microscopy was carried out to assess the penetration of the control (phosphate-buffered saline, PBS), RB, HA-RB conjugate, UCNP/PAAm, and the UCNP/PAAm/HA-RB conjugate complex delivered through the incision of *ex vivo* porcine skin (Figure 4c). The HA-RB conjugate was deeply delivered from the surface of the incision compared with the RB. While UCNP/PAAm was not found much in the tissue, UCNP/PAAm complexed with the HA-RB conjugate was highly detected at the incision. All these results confirmed the effective green light delivery of UCNPs into the incised porcine skin tissue.

Two-Photon Microscopy for the Transdermal Delivery *in Vivo*. *In vivo* transdermal delivery of the UCNP/PAAm/HA-RB conjugate complex was investigated by two-photon microscopy. After removal of hair, each group was treated by topical administration of RB, the HA-RB conjugate, UCNP/PAAm, and the UCNP/PAAm/HA-RB conjugate complex onto the dorsal skin of BALB/c mice (6 weeks old) for 30 min. Then, mice were sacrificed and the skin tissues were collected for two-photon fluorescence microscopy to visualize the particle distribution in the skin tissue (Figure 5). The yellow fluorescence corresponds to RB at 1050 nm and green fluorescence indicates UCNP/PAAm at 900 nm. The HA-RB conjugate was delivered through the skin and observed in yellow in the epidermis and the collagen layer, whereas RB mainly remained on the subcutaneous layer as reported elsewhere.[24] Upon illumination of a 900 nm two-photon laser, UCNP/PAAm showed green fluorescence in the collagen layer. The penetration of UCNP/PAAm into the deep tissue might be ascribed to the small size of the nanoparticles.[25] Moreover, both the HA-RB conjugate and UCNP/PAAm/HA-RB conjugate complex were observed in the collagen layer of

DOI: 10.1021/acsnano.7b04153
ACS Nano 2017, 11, 9979−9988

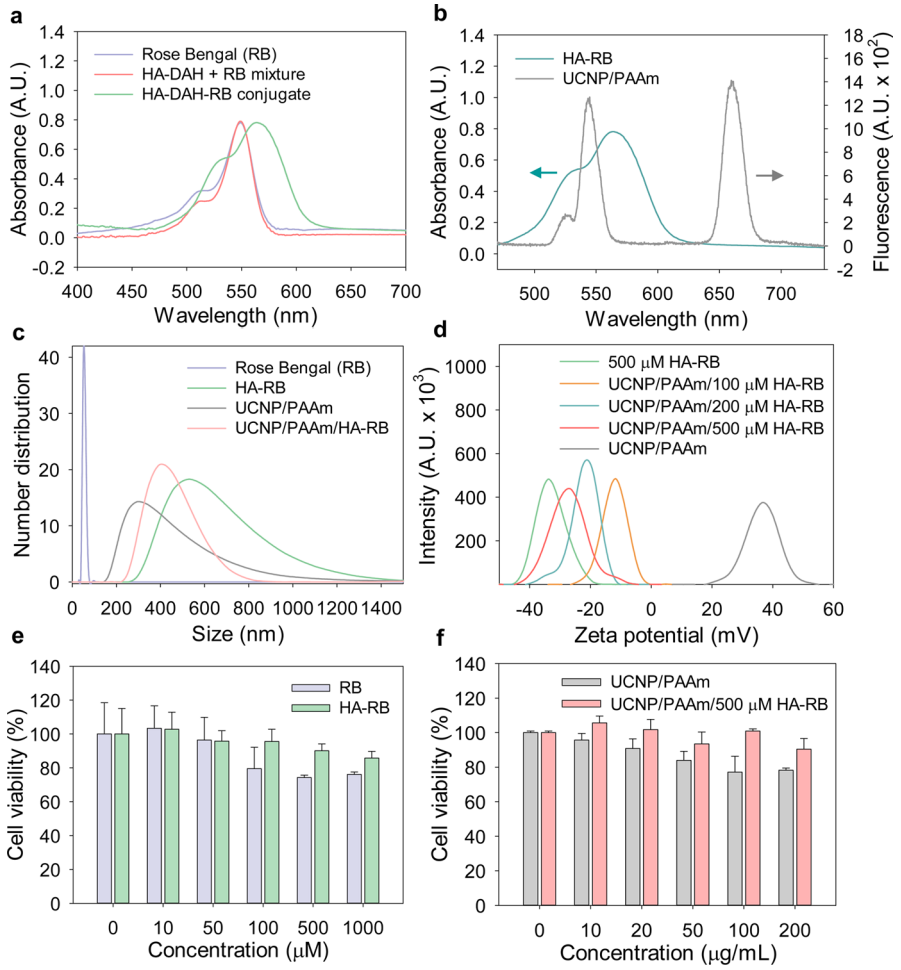

Figure 3. Characterization and biocompatibility assessment of the UCNP/PAAm/HA-RB conjugate complex. (a) Absorbance spectra of RB, a mixture of HA-diaminohexane (DAH) and RB, and HA-DAH-RB (HA-RB) conjugate. (b) UCNP fluorescence excited at 980 nm and the absorbance of HA-RB conjugate. (c) The size distribution and (d) the zeta potential of RB, HA-RB conjugate, UCNP/PAAm, and UCNP/PAAm/HA-RB conjugate complex. The cytocompatibility of (e) RB and HA-RB conjugate, (f) UCNP/PAAm and UCNP/PAAm/HA-RB conjugate complex in NIH3T3 cells by the MTT assay (n = 4). Data are expressed as mean ± SD.

the epidermis and dermis. From the results, HA appeared to enhance the transdermal penetration of conjugated or complexed materials from the subcutaneous to the dermal layer.[26,27]

Collagen Fibrillogenesis for Photochemical Tissue Bonding. The kinetics and degree of collagen fibrillogenesis were assessed by spectrophotometrically measuring the turbidity of collagen solutions (Figure 6a). Each sample of the control (DI water), RB, HA-RB conjugate, and UCNP/PAAm/HA-RB conjugate complex was added into the neutralized collagen type 1 solution on ice. The absorbance at 315 nm was measured every 1 min for 30 min with 980 nm NIR light illumination at 37 °C in the temperature-controlled microplate spectrophotometer. As shown in Figure 6a, the UCNP/PAAm/HA-RB conjugate complex resulted in the rapid optical density increase reflecting the collagen cross-linking, compared with the control, RB, and HA-RB conjugate under NIR light illumination (*ca.* 500 mW/cm^2). Figure 6b shows the collagen fibrillogenesis rate determined from the slope of the curve in Figure 6a. The collagen fibrillogenesis rate increased significantly for the case of the UCNP/PAAm/HA-RB conjugate complex with 980 nm NIR light illumination. From the results, we could confirm that UCNP triggered by NIR light activated the RB in the HA-RB conjugate and induced the accelerated collagen cross-linking.

***Ex Vivo* Collagen Cross-Linking in the Porcine Skin.** The collagen cross-linking in the porcine skin was assessed by measuring the tensile strength of adhered skin with a universal testing machine. As schematically shown in Figure 6c, 2 pieces of porcine skins (1 cm × 10 cm) were used as tissue substrates, and the bonding area was fixed with a transparent acrylic fixture. After that, PBS and the UCNP/PAAm/HA-RB conjugate complex were loaded on the bonding site (1 cm × 1 cm) between the porcine skins. The tissue specimens were illuminated with NIR light for 20 min to cross-link the collagen matrix by the activated HA-RB conjugate under the green fluorescence of UCNP in the complex. The bonded tissue specimens were strained with a 10 N load cell until complete separation at a speed of 5 mm/min. As shown in Figure 6d, the skin tissue treated by the control (PBS) and UCNP/PAAm/HA-RB conjugate complex without NIR light illumination showed a low tensile strength of 7.09 ± 1.24 and 5.38 ± 0.06 kPa, respectively. On the other hand, the NIR light-illuminated skin after treatment with the UCNP/PAAm/HA-RB conjugate complex was tightly bonded by the collagen cross-linking with a high tensile strength of 17.57 ± 2.42 kPa. The light treatment

DOI: 10.1021/acsnano.7b04153
ACS Nano 2017, 11, 9979−9988

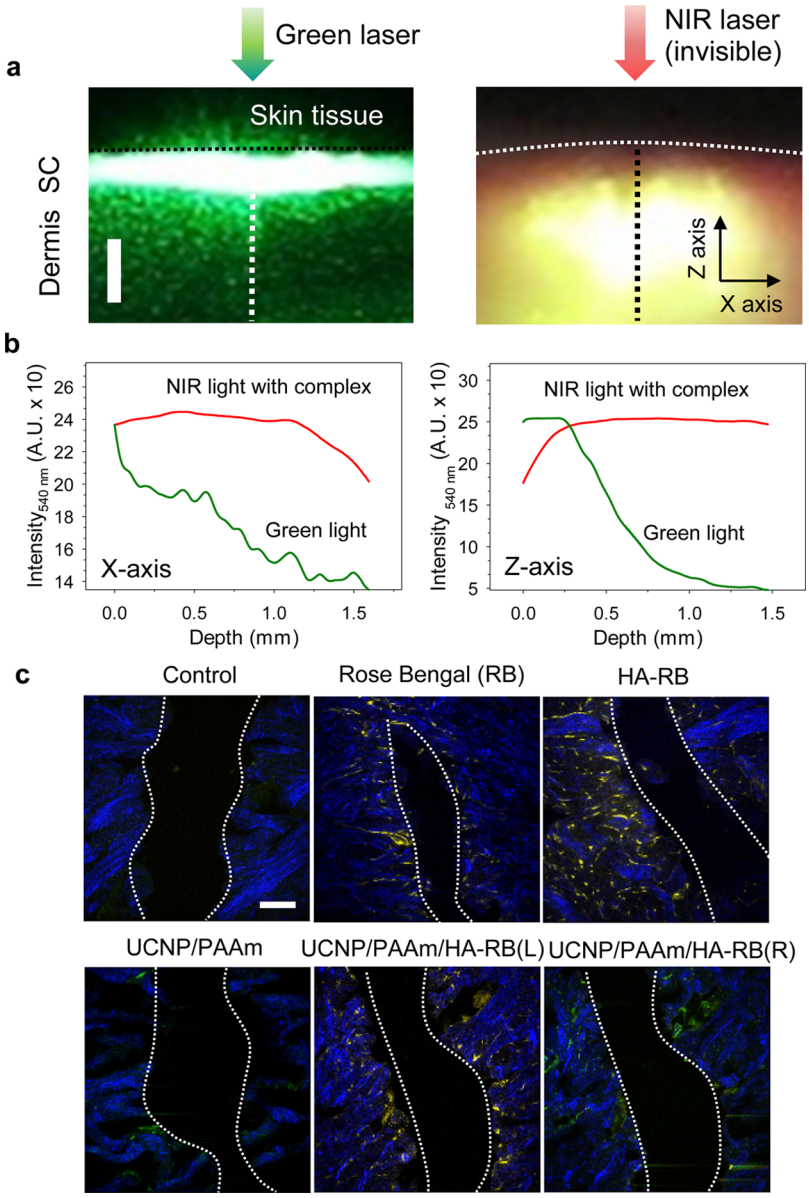

Figure 4. Light propagation in the incision of porcine skin tissue. (a) Propagation of green light (left) and light converted by the UCNP/PAAm/HA-RB conjugate complex upon invisible NIR light illumination (right). The invisible NIR laser is directly illuminated to the incision area treated with the UCNP/PAAm/HA-RB conjugate complex (scale bar = 1 mm). Dashed lines indicate the incision and the surface of skin. (b) Green fluorescence profile in the skin tissue treated with green light (green) or with the UCNP/PAAm/HA-RB conjugate complex and NIR light illumination (red) in *X*- and *Z*-axes. (c) *Ex vivo* two-photon microscopic images after topical delivery of the samples to the incision of porcine skin (L: the fluorescence of HA-RB conjugate, R: the fluorescence of UCNP, blue = collagen, yellow = RB, green = UCNP, scale bar = 100 μm).

with PBS as a control also showed a slight tissue bonding effect with a tensile strength of 12.45 ± 0.21 kPa (Figure 6d).

***In Vivo* PTB by the UCNP/PAAm/HA-RB Conjugate Complex under NIR Light Illumination.** The effect of the UCNP/PAAm/HA-RB conjugate complex on PTB *in vivo* was investigated on the dorsal skin of mice. After making an incision, the dorsal skin was treated with (i) the control (PBS), (ii) PBS and an NIR laser, (iii) the UCNP/PAAm/HA-RB conjugate complex, (iv) the HA-RB conjugate and a green laser, (v) the positive control of suturing, and (vi) the UCNP/PAAm/HA-RB conjugate complex and an NIR laser, respectively. The resulting tissue bonding was observed at the predetermined time point (Figure 7a). Figure 7b shows photoimages for the tissue bonding at day 0, 1, and 3 by the above treatment for six groups. According to the visual analysis, the UCNP/PAAm/HA-RB conjugate complex with NIR light illumination showed the fastest tissue bonding, followed by the HA-RB conjugate with green light and PBS with NIR light, sequentially. Although all wounds were not healed completely at day 3 due to the free movement of mice, we could find the difference in the tissue bonding status. There were scabs in the wound that had been spread for the case of the untreated control and the UCNP/PAAm/HA-RB conjugate complex without NIR light illumination (Figure 7b). The wound seemed to be well-bonded in the case of suturing, but there were scars passed by the surgical threads.

The PTB effect of the UCNP/PAAm/HA-RB conjugate complex was also assessed by measuring the tensile strength of

DOI: 10.1021/acsnano.7b04153
ACS Nano 2017, 11, 9979−9988

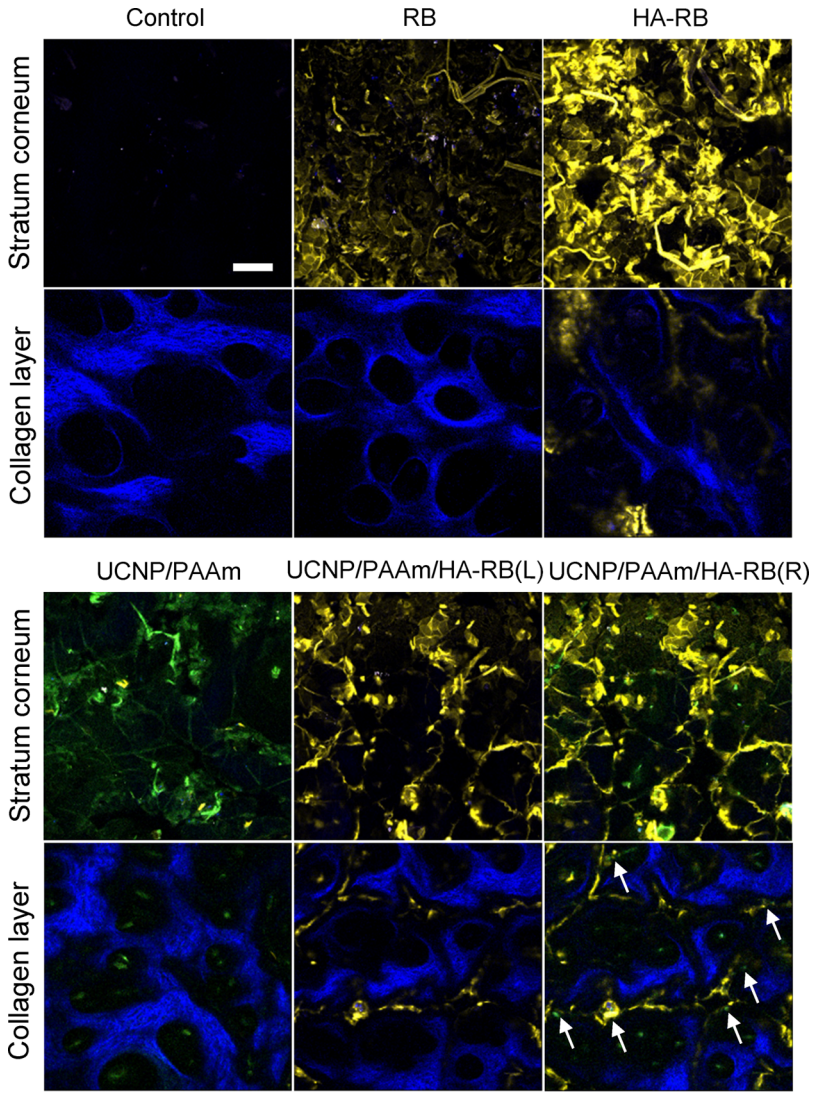

Figure 5. Two-photon microscopy for *in vivo* transdermal delivery. Two-photon microscopic images for the dorsal skin of BALB/c mice after transdermal delivery of the control (PBS), RB, HA-RB conjugate, UCNP/PAAm, and UCNP/PAAm/HA-RB conjugate complex (L: the fluorescence of HA-RB conjugate, R: the merged fluorescence) (blue = collagen, yellow = RB, green = UCNP, scale bar = 100 μm). White arrows indicate the merged fluorescence of UCNP and the HA-RB conjugate in the complex.

dissected skin tissues (Figure 7c). The untreated control and the UCNP/PAAm/HA-RB conjugate complex without NIR laser groups showed a relatively low tensile strength of 5.68 ± 3.63 and 7.33 ± 4.81 kPa, respectively. The tensile strength of skin tissues treated with the HA-RB conjugate and green light was 16.80 ± 5.50 kPa, and that of the UCNP/PAAm/HA-RB conjugate complex with NIR light illumination showed the highest tensile strength of 35.07 ± 2.75 kPa. Although conventional suturing also resulted in the relatively high tensile strength of 22.40 ± 3.90 kPa, it was still lower than that of the UCNP/PAAm/HA-RB conjugate complex with NIR light illumination. The NIR light treatment also slightly increased the tensile strength to the value of 14.13 ± 5.40 kPa, which was statistically higher than that of the untreated control. Taken together, we could confirm the feasibility of the UCNP/PAAm/HA-RB conjugate complex for the futuristic light-triggered facile tissue bonding.

The advantageous features of PTB include a water-tight closure across the entire wound interface with minimal scar formation, compared with the invasive standard suturing and stapling or tissue bonding with cyanoacrylate and fibrin glues. However, the application of PTB with green light illumination has been limited to superficial wounds with a maximum depth of 1−2 mm.[4] In contrast, the UCNP/PAAm/HA-RB conjugate complex could be successfully applied to the photochemical bonding of deep tissue with NIR light illumination. Recently, silica nanoparticles have been developed for the adhesion of tissues acting as connectors between polymer chains or wound tissues.[28,29] However, the PTB protocol using the UCNP/PAAm/HA-RB conjugate complex might be more clinically feasible with NIR light illumination. This futuristic system can be harnessed for robot surgery with facile and quick tissue bonding triggered by light illumination.

CONCLUSIONS

We successfully demonstrated the feasibility of the UCNP/PAAm/HA-RB conjugate complex for noninvasive PTB in deep tissue under NIR light illumination. HA in the conjugate appeared to facilitate the penetration of RB into a deep and wide area from the boundary of incision. UCNPs in the

DOI: 10.1021/acsnano.7b04153
ACS Nano 2017, 11, 9979−9988

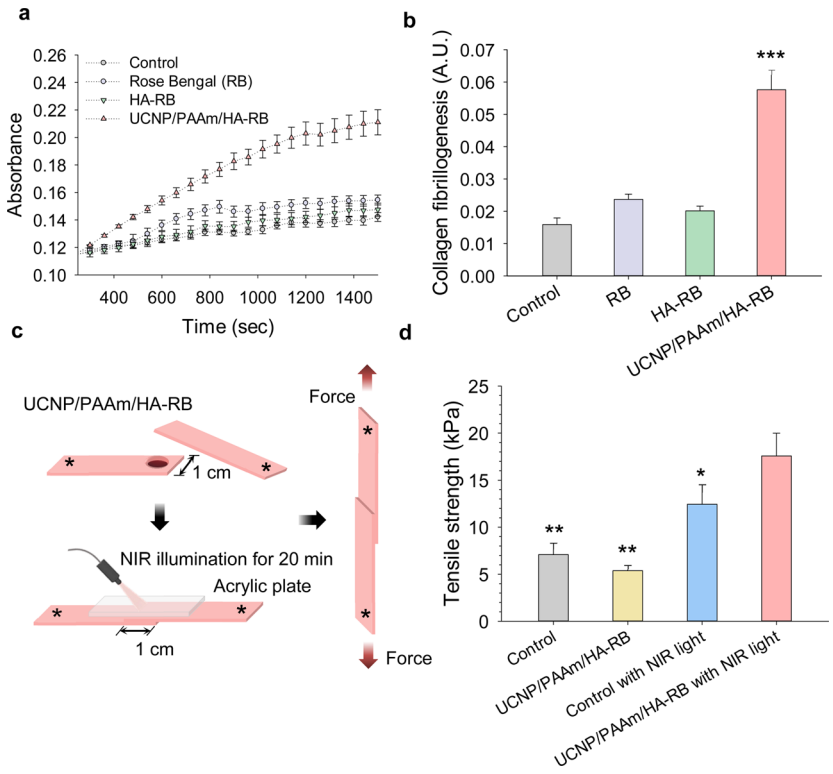

Figure 6. Collagen fibrillogenesis and *ex vivo* tensile strength. (a) Degree of collagen cross-linking determined by measuring the absorbance of type 1 collagen at 315 nm after treatment with DI water, RB, HA-RB conjugate, and UCNP/PAAm/HA-RB conjugate complex for 30 min followed by NIR light illumination. (b) Collagen fibrillogenesis rate after treatment with the samples in (a) (n = 4, ***P < 0.001 *versus* the others). (c) Schematic illustration for *ex vivo* tensile strength test to assess the photochemical tissue bonding of porcine skin. (d) Tensile strength of adhered tissues by the treatment of the control (PBS), UCNP/PAAm/HA-RB conjugate complex, PBS with NIR light illumination, and UCNP/PAAm/HA-RB conjugate complex with NIR light illumination (n = 3, *P < 0.05, **P < 0.01, ***P < 0.001 *versus* UCNP/PAAm/HA-RB conjugate complex with NIR light).

complex showed the effective light-guiding ability into the deep tissue as an alternative to implantable or injectable light-guiding materials. Two-photon microscopy revealed the facilitated transdermal delivery of the complex into the dermal tissue. After confirming *in vitro* collagen fibrillogenesis, we performed *ex vivo* and *in vivo* skin tissue bonding, which revealed the photochemically accelerated tissue bonding effect of the UCNP/PAAm/HA-RB conjugate complex under noninvasive NIR light illumination. The UCNP/PAAm/HA-RB conjugate complex resulted in a higher tensile strength than that of the conventional suturing without allergic side effects. This platform technology of the UCNP/PAAm/HA-RB conjugate complex might be successfully applied for the development of various futuristic photomedicines.

MATERIALS AND METHODS

Materials. Yttrium(III) chloride hexahydrate ($YCl_3{\cdot}6H_2O$), ytterbium(III) chloride hexahydrate ($YbCl_3{\cdot}6H_2O$), erbium chloride hexahydrate ($ErCl_3{\cdot}6H_2O$), octadecene-1, ammonium fluoride (NH_4F), cyclohexane, poly(allylamine) solution (MW = 17 kDa, 20 wt % in H_2O), dimethyl sulfoxide (DMSO), diaminohexane (DAH), *N*-hydroxysuccinimide sodium salt (NHS), collagen from rat tail, and 2-[4-(2-hydroxyethyl)piperazin-1-yl]ethanesulfonic acid (HEPES) buffer solution were purchased from Sigma-Aldrich (St. Louis, MO, USA). Oleic acid and 1-ethyl-3-(3-(dimethylamino)propyl)-carbodiimide hydrochloride (EDC) were obtained from Tokyo Chemical Industry (Tokyo, Japan). Sodium hydroxide (NaOH) was acquired from Samchun Pure Chemicals (Seoul, Korea). Hyaluronate (MW 100 kDa) was purchased from Lifecore Biomedical (Chaska, MN, USA). Rose bengal (RB) dye was purchased from Junsei Chemical Co. (Tokyo, Japan). 3-(4,5-Dimethylthiazol-2-yl)-2,5-diphenyltetrazolium bromide (MTT) was purchased from Promega (Madison, WI, USA), and PBS (pH 7.4) was obtained from Tech & Innovation (Seoul, Korea). Dulbecco's modified Eagle's medium (DMEM), fetal bovine serum (FBS), and antibiotics were purchased from Gibco (Grand Island, NY, USA). A mouse embryonic fibroblast of the NIH3T3 cell line was obtained from American Type Culture Collection (ATCC) (Manassass, VA, USA).

Synthesis of UCNP and the UCNP/PAAm. Upconversion nanoparticles of $NaYF_4$:Yb/Er (Y:Yb:Er = 78:20:2) were prepared using an aqueous solution of $LnCl_3{\cdot}6H_2O$ [0.78 mL of $YCl_3{\cdot}6H_2O$ (1 M), 0.2 mL of $YbCl_3{\cdot}6H_2O$ (1 M), 0.2 mL of $ErCl_3{\cdot}6H_2O$ (0.1 M)] in a 250 mL three-neck flask as reported elsewhere.[30,31] The flask was fitted in a 250 mL spherical heating mantle and heated to 110 °C to evaporate water from $LnCl_3{\cdot}xH_2O$ with magnetic stirring at 350 rpm. Then, 6 mL of oleic acid and 15 mL of 1-octadecene were added, which was heated to 150 °C for 30 min to obtain a homogeneous solution. After cooling to 60 °C, NH_4F (0.148 g) and NaOH (0.1 g) dissolved in 5 mL of methanol solution was added to the solution dropwise. The mixture was heated to 110 °C and kept over 20 min to evaporate methanol and residual H_2O. The neck of the flask was blocked with a rubber stopper and sealed with a paraffin film. Then, a nitrogen-filled balloon with a syringe was connected through a rubber stopper for pressure stabilization. The other neck of the flask was plugged to a dual manifold Schlenk line so that the solution was kept in the vacuum for 10 min and filled with nitrogen by turning the stopcock. The solution was heated to 300 °C at a heating rate of 10 °C/min, and the temperature was maintained under nitrogen for 1 h with vigorous stirring. The mixture was cooled to room temperature and transferred to a 50 mL conical tube after washing the flask with 40 mL of acetone to collect the remaining product. The tube containing the solution was centrifuged at 6654*g* and 20 °C for 10 min. After

DOI: 10.1021/acsnano.7b04153
ACS Nano 2017, 11, 9979−9988

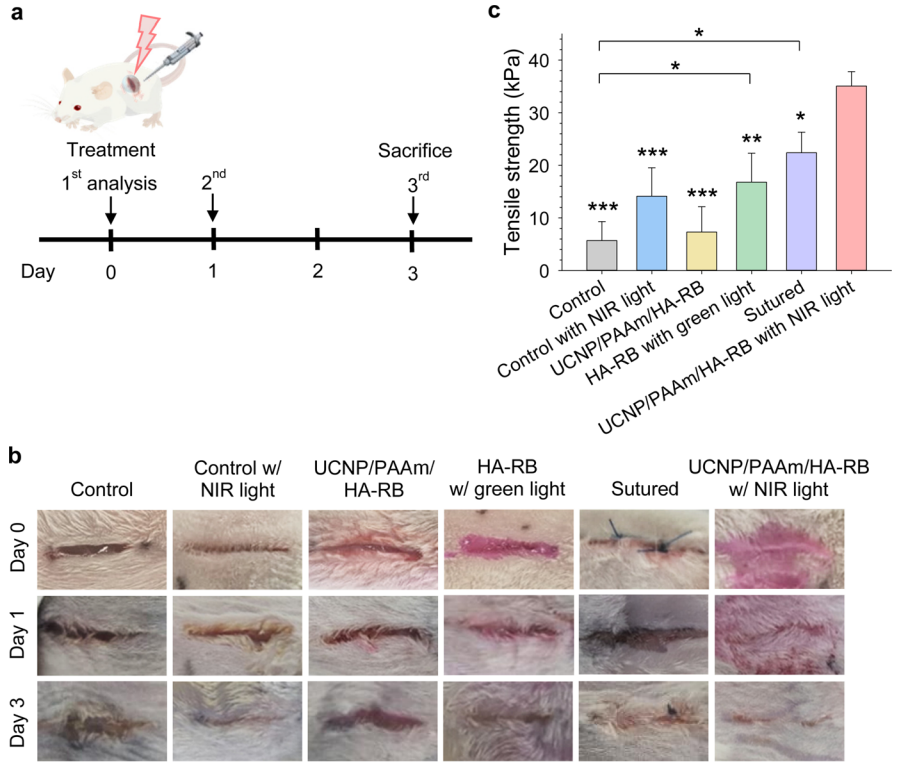

Figure 7. ***In vivo*** **photochemical tissue bonding (PTB) and the resulting tensile strength. (a) Schematic illustration for** ***in vivo*** **PTB test with three analyses before sacrifice for tensile strength test. (b) Photoimages for the incised dorsal skin of BALB/c mice treated with the control (PBS), PBS and NIR light, the UCNP/PAAm/HA-RB conjugate complex, the HA-RB conjugate and green light, suturing, and the UCNP/PAAm/HA-RB conjugate complex and NIR light at day 0, 1, and 3. (c)** ***In vivo*** **tensile strength of the six groups at day 3 (n = 3, *P < 0.05, **P < 0.01, ***P < 0.001** ***versus*** **UCNP/PAAm/HA-RB conjugate complex with NIR light).**

removing the supernatant, the pellet was dissolved in 20 mL of cyclohexane. The solution was centrifuged again at 1000g and 20 °C for 5 min, and the supernatant containing UCNP was collected in a 40 mL of glass vial. The surface of hydrophobic UCNPs was modified with PAAm by ligand exchange as reported elsewhere.[32,33] The PAAm solution (10 μL, 20 wt % in H_2O) was dissolved in 4 mL of ethanol and sonicated for 20 min. The solution of hydrophobic UCNPs (*ca.* 4 mg) in 2 mL of cyclohexane was added dropwise to the PAAm solution, which was vigorously mixed at room temperature for 36 h. The obtained UCNP/PAAm was centrifuged at 10400g and 20 °C for 20 min and redispersed in DI water.

Preparation of the UCNP/PAAm/HA-RB Conjugate Complex. First, the HA-RB conjugate was synthesized by the coupling reaction of HA-DAH with RB. HA-DAH with a DAH content of 20 mol % was synthesized by the reaction between HA (100 kDa, 500 mg) and DAH (2.89 g, 20 molar ratio to HA) in sodium acetate buffer (pH 4.8) for 5 min using the EDC chemistry. RB was added into the HA-DAH (20%) solution at a molar ratio of 1:2 (DAH:RB), which was mixed with a 10 molar excess of EDC and NHS, maintaining the pH at 4.8 with 1 M HCl and 1 M NaOH solutions over 30 min. The mixture stirred in the dark at room temperature for 12 h. Then, the HA-RB conjugate was purified by dialysis against DI water (MWCO = 10 kDa). The powder of the HA-RB conjugate was obtained by freeze-drying for 3 days and stored in the dark until further use. After that, the UCNP/PAAm/HA-RB conjugate complex was prepared by simple mixing of 500 μM HA-RB conjugate and 200 μg/mL of UCNP/PAAm.

Characterization of the UCNP/PAAm/HA-RB Conjugate Complex. The prepared HA-RB conjugate, UCNP/PAAm, and the UCNP/PAAm/HA-RB conjugate complex were analyzed by TEM (JEM-1011, JEOL Co., Akishima, Japan), HRTEM (JEM-2200FS with Cs-corrected TEM, JEOL Co., Akishima, Japan), EDS (JEM-2200FS, JEOL Co., Akishima, Japan), DLS (Zetasizer Nano ZS90, Malvern Instruments Co., Malvern, UK), and UV/vis spectrophotometry (S-3100, Scinco Co., Seoul, Korea). The core structure and uniform crystal lattice of UCNPs were analyzed by TEM and HRTEM, and the composition of the UCNPs was determined by EDS. The surface modification of the UCNPs with PAAm was analyzed by TEM and DLS. The fluorescence of UCNP and UCNP/PAAm was analyzed with a Fluorolog modular spectrofluorometer (FL-1039, Horiba Scientific Co., Kyoto, Japan) with excitation at 980 nm. The synthesized HA-RB conjugate was analyzed by UV/vis spectrophotometry and the formation of the UCNP/PAAm/HA-RB conjugate complex was analyzed by DLS.

In Vitro **Cytotoxicity Test.** The cytotoxicity of HA-RB conjugate, UCNP/PAAm, and the UCNP/PAAm/HA-RB conjugate complex was assessed in NIH3T3 cells using the MTT assay. Briefly, the cryopreserved NIH3T3 cells were seeded in a 75T flask with DMEM for a day and transferred into 96-well plates at a density of 5×10^4 cells per well. The cells were incubated with the control (medium), UCNP/PAAm, RB, HA-RB conjugate, and UCNP/PAAm/HA-RB conjugate complex at 37 °C and 5% CO_2 for a day (n = 4). After incubation for 24 h, NIH3T3 cells were washed with PBS twice and the medium in each well was replaced with 50 μL of MTT solution (5 mg/mL). When the purple precipitates were visible in 1 h, the solution of each well was aspirated and 100 μL of DMSO was added to dissolve the formazan crystal. The optical density at 540 nm was measured with a microplate spectrophotometer (EMax End point ELISA microplate reader, Molecular Devices, CA, USA). The cell viability (%) was calculated using the following equation: $[A_{540\ (sample)}/A_{540\ (control)}] \times 100$, where $A_{540\ (sample)}$ is the optical density of the sample-treated wells and $A_{540\ (control)}$ is that of serum-free medium-treated wells.

Light Propagation Assessment into Closed Incision of Porcine Tissue. The porcine skin was prepared with the dimensions of 2 cm × 1 cm × 0.2 cm (length × width × height) and incised. Then, 50 μL of the UCNP/PAAm/HA-RB conjugate complex was loaded in the incision for 30 min. After removal, a green laser (540 nm) and an NIR laser (980 nm) were illuminated onto the closed incision. The

DOI: 10.1021/acsnano.7b04153
ACS Nano 2017, 11, 9979−9988

front cross-section was visualized by microscopy (Canon EOS 100D, Canon, Tokyo, Japan). The profile of the green fluorescence in the microscopic image was analyzed by ImageJ software. In addition, each 50 μL of the control (PBS), HA-RB conjugate (500 μM), and UCNP/PAAm/HA-RB conjugate complex was delivered through the 1 cm incision on 2 × 2 cm^2 dissected porcine skin for 30 min. After the porcine skin was washed with PBS, the penetration depth of the samples from the boundary of the incision was analyzed by two-photon microscopy after cryo-sectioning and tissue fixation.

***In Vivo* Transdermal Delivery Test.** An *in vivo* transdermal delivery test was performed by topical administration of each 50 μL of the control (PBS), HA-RB conjugate (500 μM), and UCNP/PAAm/HA-RB conjugate complex onto the 1 × 1 cm^2 dorsal skin of 6-week-old BALB/c mice. After transdermal delivery for 30 min, the treated tissues were dissected and washed with PBS. The penetration depth of samples into the skin was analyzed by two-photon microscopy with excitation at 900 and 1050 nm. All animal experiments were performed following the laboratory animal protocol approved by the institutional animal care and use committee of the Pohang University of Science and Technology in accordance with the National Institutes of Health Guide for the Care and Use of Experimental Animals.

Collagen Fibrillogenesis Test. Collagen fibrillogenesis test was carried out as described elsewhere.[34,35] The rate and extent of collagen cross-linking was assessed spectrophotometrically. The type 1 collagen from rat tail was dissolved at a concentration of 3.0 mg/mL in 20 mM acetic acid and neutralized on ice with 0.2 M HEPES and 10× PBS in a volume ratio of 8:1:1, respectively. The aqueous solution of DI water, RB, 500 μM HA-RB conjugate, or UCNP/PAAm/HA-RB conjugate complex was added into the neutralized collagen solution, and then 200 μL of the mixture was transferred into the 96-well microplate (n = 4). The absorbance from 315 to 405 nm was measured per 1 min for 30 min with NIR light illumination (*ca.* 500 mW/cm^2) at 37 °C in a temperature-controlled microplate spectrophotometer.

***Ex Vivo* Tensile Strength Test.** *Ex vivo* tensile strength of porcine skin was measured by using a universal testing machine (Instron 3340, Instron Co., Norwood, MA, USA) equipped with a 10 N load cell.[36] The porcine skin was prepared as a tissue substrate with a size of 1 × 10 cm^2, whose bonding area was 1 × 1 cm^2. Each 50 μL of the control (PBS), UCNP/PAAm/HA-RB conjugate complex, PBS with NIR laser (500 mW/cm^2), and UCNP/PAAm/HA-RB conjugate complex with NIR light (NIR light = 500 mW/cm^2, green light converted from NIR by UCNP = 1.5 mW/cm^2) was loaded on the 1 × 1 cm^2 surface of the prepared porcine skin, and the tissue specimen was covered with another specimen. The two-layered tissue substrates were fixed with a transparent acrylic plate and Scotch tape and then immediately illuminated with a 980 nm NIR laser for 20 min (n = 3). After light treatment, the specimens were stored in humid conditions at room temperature for 1 h prior to the tensile strength measurement. The adhered specimens were loaded on the Instron and pulled at a crosshead speed of 5 mm/min until complete separation. The data from the specimens (n = 3) were averaged for the tensile strength.

***In Vivo* Tissue Bonding Test.** The *in vivo* tissue bonding test was carried out to assess the tissue bonding effect of the UCNP/PAAm/HA-RB conjugate complex upon NIR light illumination. Normal 6-week-old BALB/c mice were anesthetized and shaved, and then a 1 cm incision was made on the deep tissue of the dorsal skin in the mice. The incised dorsal skins were treated with 50 μL of the control (PBS), PBS with NIR light, UCNP/PAAm/HA-RB conjugate complex, HA-RB conjugate with green light, the suturing, and UCNP/PAAm/HA-RB conjugate complex with NIR light for 20 min (NIR light = 500 mW/cm^2, green light converted by UCNP = 1.5 mW/cm^2 and green light = 7.5 mW/cm^2). Each incised dorsal skin was observed at 3 time points of day 0, day 1, and day 3, and the treated skins (1 × 1 cm^2) were collected and used for the tensile strength test after CO_2 euthanization. The treated tissue specimens were cut at an average size of 1 × 2 cm^2 and stored in humid conditions with a PBS-soaked gauze for 1 h. The adhered skin tissues were tested on the Instron with a 10 N load cell at a crosshead speed of 5 mm/min until complete separation.

Statistical Analysis. Statistical analysis was performed *via* the one-way ANOVA using the software SigmaPlot 12.0. (Systat Software Inc., San Jose, CA, USA). The values of $^*P < 0.05$, $^{**}P < 0.01$, and $^{***}P < 0.001$ were determined as statistically significant. Data were expressed as means ± standard deviation (SD) from several separate experiments.

AUTHOR INFORMATION

Corresponding Authors

*Tel: +82 54 279 8805. Fax: +82 54 279 2399. E-mail: kskim1127@gmail.com (K. S. Kim).

*Tel: +82 54 279 2159. Fax: +82 54 279 2399. E-mail: skhanb@postech.ac.kr (S. K. Hahn).

ORCID

Sei Kwang Hahn: 0000-0002-7718-6259

Present Address

[‖]Department of Organic Materials Science and Engineering, School of Engineering, Pusan National University, 2 Busandaehak-ro 63 beon-gil, Geunjeong, Busan, 46241, Korea.

Notes

The authors declare no competing financial interest.

ACKNOWLEDGMENTS

This research was supported by the Nano·Material Technology Development Program (No. 2017M3A7B8065278), the Basic Science Research Program (No. 2017R1E1A1A03070458), and the Center for Advanced Soft-Electronics (Global Frontier Project, CASE-2015M3A6A5072945) through the National Research Foundation of Korea (NRF) funded by the Ministry of Science, ICT and Future Planning.

REFERENCES

(1) Barton, M.; Piller, S. C.; Mahns, D. A.; Morley, J. W.; Mawad, D.; Longo, L.; Lauto, A. *In Vitro* Cell Compatibility Study of Rose Bengal-Chitosan Adhesives. *Lasers Surg. Med.* **2012**, *44*, 762−768.

(2) Johnson, T. S.; O'Neill, A. C.; Motarjem, P. M.; Amann, C.; Nguyen, T.; Randolph, M. A.; Winograd, J. M.; Kochevar, I. E.; Redmond, R. W. Photochemical Tissue Bonding: A Promising Technique for Peripheral Nerve Repair. *J. Surg. Res.* **2007**, *143*, 224−229.

(3) Tsao, S.; Yao, M.; Tsao, H.; Henry, F. P.; Zhao, Y.; Kochevar, J. J.; Redmond, R. W.; Kochevar, I. E. Light-Activated Tissue Bonding for Excisional Wound Closure: A Split-Lesion Clinical Trial. *Br. J. Dermatol.* **2012**, *166*, 555−563.

(4) Nizamoglu, S.; Gather, M. C.; Humar, M.; Choi, M.; Kim, S.; Kim, K. S.; Hahn, S. K.; Scarcelli, G.; Randolph, M.; Redmond, R. W.; Yun, S. H. Bioabsorbable Polymer Optical Waveguides for Deep-Tissue Photomedicine. *Nat. Commun.* **2016**, *7*, 10374.

(5) Wang, F.; Han, Y.; Lim, C. S.; Lu, Y.; Wang, J.; Xu, J.; Chen, H.; Zhang, C.; Hong, M.; Liu, X. Simultaneous Phase and Size Control of Upconversion Nanocrystals through Lanthanide Doping. *Nature* **2010**, *463*, 1061−1065.

(6) Dong, H.; Du, S. R.; Zheng, X. Y.; Lyu, G. M.; Sun, L. D.; Li, L. D.; Zhang, P. Z.; Zhang, C.; Yan, C. H. Lanthanide Nanoparticles: From Design toward Bioimaging and Therapy. *Chem. Rev.* **2015**, *115*, 10725−10815.

(7) Lu, Y.; Zhao, J.; Zhang, R.; Liu, Y.; Liu, D.; Goldys, E. M.; Yang, X.; Xi, P.; Sunna, A.; Lu, J.; Shi, Y.; Leif, R. C.; Huo, Y.; Shen, J.; Piper, J. A.; Robinson, P.; Jin, D. Tunable Lifetime Multiplexing Using Luminescent Nanocrystals. *Nat. Photonics* **2014**, *8*, 32−36.

(8) Niu, W.; Wu, S.; Zhang, S.; Li, L. Synthesis of Colour Tunable Lanthanide-Ion Doped $NaYF_4$ Upconversion Nanoparticles by Controlling Temperature. *Chem. Commun.* **2010**, *46*, 3908−3910.

DOI: 10.1021/acsnano.7b04153
ACS Nano 2017, 11, 9979−9988

(9) Hong, G.; Lee, J. C.; Robinson, J. T.; Raaz, U.; Xie, L.; Huang, N. F.; Cooke, J. P.; Dai, H. Multifunctional *In Vivo* Vascular Imaging Using Near-Infrared II Fluorescence. *Nat. Med.* **2012**, *18*, 1841−1848.
(10) Cheng, L.; Yang, K.; Li, Y.; Zeng, X.; Shao, M.; Lee, S. T.; Liu, Z. Multifunctional Nanoparticles for Upconversion Luminescence/MR Multimodal Imaging and Magnetically Targeted Photothermal Therapy. *Biomaterials* **2012**, *33*, 2215−2222.
(11) Idris, N. M.; Gnanasammandhan, M. K.; Zhang, J.; Ho, P. C.; Mahendran, R.; Zhang, Y. *In Vivo* Photodynamic Therapy Using Upconversion Nanoparticles as Remote-Controlled Nanotransducers. *Nat. Med.* **2012**, *18*, 1580−1585.
(12) Wang, C.; Tao, H.; Cheng, L.; Liu, Z. Near-Infrared Light Induced *In Vivo* Photodynamic Therapy of Cancer Based on Upconversion Nanoparticles. *Biomaterials* **2011**, *32*, 6145−6154.
(13) Zhu, X.; Feng, W.; Chang, J.; Tan, Y. W.; Li, J.; Chen, M.; Sun, Y.; Li, F. Temperature-Feedback Upconversion Nanocomposite for Accurate Photothermal Therapy at Facile Temperature. *Nat. Commun.* **2016**, *7*, 10437.
(14) Kong, W. H.; Sung, D. K.; Kim, H.; Yang, J.; Lee, J.; Kim, D.; Hahn, S. K. Self-Adjuvanted Hyaluronate-Antigenic Peptide Conjugate for Transdermal Treatment of Muscular Dystrophy. *Biomaterials* **2016**, *81*, 93−103.
(15) Jung, H. S.; Kong, W. H.; Sung, D. K.; Lee, M. Y.; Beack, S. E.; Keum, D. H.; Kim, K. S.; Yun, S. H.; Hahn, S. K. Nanographene Oxide-Hyaluronic Acid Conjugate for Photothermal Ablation Therapy of Skin Cancer. *ACS Nano* **2014**, *8*, 260−268.
(16) Beack, S.; Kong, W. H.; Jung, H. S.; Do, I. H.; Han, S.; Kim, H.; Kim, K. S.; Yun, S. H.; Hahn, S. K. Photodynamic Therapy of Melanoma Skin Cancer Using Carbon Dot-Chlorin E6-Hyaluronate Conjugate. *Acta Biomater.* **2015**, *26*, 295−305.
(17) Kim, H.; Jeong, H.; Han, S.; Beack, S.; Hwang, B. W.; Shin, M.; Oh, S. S.; Hahn, S. K. Hyaluronate and Its Derivatives for Customized Biomedical Applications. *Biomaterials* **2017**, *123*, 155−171.
(18) Boyer, J. C.; Veggel, F. C. J. M. Absolute Quantum Yield Measurements of Colloidal $NaYF_4$:Er^{3+},Yb^{3+} Upconverting Nanoparticles. *Nanoscale* **2010**, *2*, 1417−1419.
(19) Wilhelm, S.; Kaiser, M.; Wurth, C.; Heiland, J.; Carrion, C. C.; Muhr, V.; Wolfbeis, O. S.; Parak, W. J.; Genger, U. R.; Hirsch, T. Water Dispersible Upconverting Nanoparticles: Effects of Surface Modification on Their Luminescence and Colloidal Stability. *Nanoscale* **2015**, *7*, 1403−1410.
(20) Deutsch, Z.; Neeman, L.; Oron, D. Luminescence Upconversion in Colloidal Double Quantum Dots. *Nat. Nanotechnol.* **2013**, *8*, 649−653.
(21) Liu, X.; Chen, H. C.; Kong, X.; Zhang, Y.; Tu, L.; Chang, Y.; Fei, W.; Wang, T.; Reek, J. N. H.; Brouwer, A. M.; Zhang, H. Near Infrared Light-Driven Water Oxidation in a Molecule-Based Artificial Photosynthetic Device Using an Upconversion Nanophotosensitizer. *Chem. Commun.* **2015**, *51*, 13008−13011.
(22) Shrestha, A.; Hamblin, M. R.; Kishen, A. Characterization of a Conjugate between Rose Bengal and Chitosan for Targeted Antibiofilm and Tissue Stabilization Effects as a Potential Treatment of Infected Dentin. *Antimicrob. Agents Chemother.* **2012**, *56*, 4876−4884.
(23) Kim, K. S.; Kim, H.; Park, Y.; Kong, W. H.; Lee, S. W.; Kwok, S. J. J.; Hahn, S. K.; Yun, S. H. Noninvasive Transdermal Vaccination Using Hyaluronan Nanocarriers and Laser Adjuvant. *Adv. Funct. Mater.* **2016**, *26*, 2512−2522.
(24) Wachter, E.; Dees, C.; Harkins, J.; Scott, T.; Petersen, M.; Rush, R. E.; Cada, A. Topical Rose Bengal: Pre-Clinical Evaluation of Pharmacokinetics and Safety. *Lasers Surg. Med.* **2003**, *32*, 101−110.
(25) Sonavane, G.; Tomoda, K.; Sano, A.; Ohshima, H.; Terada, H.; Makino, K. *In Vitro* Permeation of Gold Nanoparticles through Rat Skin and Rat Intestine: Effect of Particle Size. *Colloids Surf., B* **2008**, *65*, 1−10.
(26) Jung, H. S.; Kim, K. S.; Yun, S. H.; Hahn, S. K. Enhancing the Transdermal Penetration of Nanoconstructs: Could Hyaluronic Acid Be the Key? *Nanomedicine* **2014**, *9*, 743−745.
(27) Kim, H.; Kong, W. H.; Seong, K. Y.; Sung, D. K.; Jeong, H.; Kim, J. K.; Yang, S. Y.; Hahn, S. K. Hyaluronate-Epidermal Growth Factor Conjugates for Skin Wound Healing and Regeneration. *Biomacromolecules* **2016**, *17*, 3694−3705.
(28) Rose, S.; Prevoteau, A.; Elziere, P.; Hourdet, D.; Marcellan, A.; Leibler, L. Nanoparticle Solutions as Adhesives for Gels and Biological Tissues. *Nature* **2014**, *505*, 382−385.
(29) Pelle, A. M.; Legrand, A.; Marcellan, A.; Louedec, L.; Letourneur, D.; Leibler, L. Organ Repair, Hemostasis, and *In Vivo* Bonding of Medical Devices by Aqueous Solutions of Nanoparticles. *Angew. Chem., Int. Ed.* **2014**, *53*, 6369−6373.
(30) Gnanasammandhan, M. K.; Idris, N. M.; Bansal, A.; Huang, K.; Zhang, Y. Near-IR Photoactivation Using Mesoporous Silica-Coated $NaYF_4$:Yb,Er/Tm Upconversion Nanoparticles. *Nat. Protoc.* **2016**, *11*, 688−713.
(31) Han, S.; Beack, S.; Jung, S. H.; Hwang, B. W.; Shin, M. H.; Kim, H.; Hahn, S. K. Hyaluronate Modified Upconversion Nanoparticles for Near Infrared Light-Triggered On-Off Tattoo Systems. *RSC Adv.* **2017**, *7*, 14805−14808.
(32) Xia, L.; Kong, X.; Liu, X.; Tu, L.; Zhang, Y.; Chang, Y.; Liu, K.; Shen, D.; Xhao, H.; Zhang, H. An Upconversion Nanoparticle−Zinc Phthalocyanine Based Nanophotosensitizer for Photodynamic Therapy. *Biomaterials* **2014**, *35*, 4146−4156.
(33) Wang, Y.; Wang, H.; Liu, D.; Song, S.; Wang, X.; Zhang, H. Graphene Oxide Covalently Grafted Upconversion Nanoparticles for Combined NIR Mediated Imaging and Photothermal/Photodynamic Cancer Therapy. *Biomaterials* **2013**, *34*, 7715−7724.
(34) Wilson, C. G.; Sisco, P. N.; Goldsmith, E. C.; Murphy, C. J. Glycosaminoglycan-Functionalized Gold Nanorods: Interactions with Cardiac Cells and Type I Collagen. *J. Mater. Chem.* **2009**, *19*, 6332−6340.
(35) Paderi, J. E.; Sistiabudi, R.; Ivanisevic, A.; Panitch, A. Collagen-Binding Peptidoglycans: A Biomimetic Approach to Modulate Collagen Fibrillogenesis for Tissue Engineering Applications. *Tissue Eng., Part A* **2009**, *15*, 2991−2999.
(36) Jeon, E. Y.; Hwang, B. H.; Yang, Y. J.; Kim, B. J.; Choi, B. H.; Jung, G. Y.; Cha, H. J. Rapidly Light-Activated Surgical Protein Glue Inspired by Mussel Adhesion and Insect Structural Crosslinking. *Biomaterials* **2015**, *67*, 11−19.

DOI: 10.1021/acsnano.7b04153
ACS Nano 2017, 11, 9979−9988